Single-Shot Edge Illumination X-ray Phase-Contrast Tomography Enabled by Joint Image Reconstruction

YUJIA CHEN[1], HUIFENG GUAN[1], CHARLOTTE K. HAGEN[2], ALESSANDRO OLIVO[2], AND MARK A. ANASTASIO[1]

[1]Department of Biomedical Engineering, Washington University in St. Louis, St. Louis, MO 63130, USA
[2]Department of Medical Physics and Biomedical Engineering, University College London, Malet Place, Gower Street, London WC1E 6BT, UK
[*]Mark A. Anastasio: anastasio@wustl.edu

Compiled November 8, 2016

Edge illumination X-ray phase-contrast tomography (EIXPCT) is an emerging X-ray phase-contrast tomography technique for reconstructing the complex-valued X-ray refractive index distribution of an object. Conventional image reconstruction approaches for EIXPCT require multiple images to be acquired at each tomographic view angle. This contributes to prolonged data-acquisition times and elevated radiation doses, which can hinder in-vivo applications. In this work, a new 'single-shot' method is proposed for joint reconstruction (JR) of the real and imaginary-valued components of the refractive index distribution from a tomographic data set that contains only a single image acquired at each view angle. The proposed method is predicated upon a non-linear formulation of the inverse problem that is solved by use of a gradient-based optimization method. The method is validated and investigated by use of computer-simulated and experimental EIXPCT data sets.

OCIS codes: *(110.7440) X-ray imaging; (110.3010) Image reconstruction techniques.*

http://dx.doi.org/10.1364/ao.XX.XXXXXX

Edge illumination X-ray phase-contrast tomography (EIXPCT) [1–3] is an emerging X-ray phase-contrast technique for reconstructing the complex-valued refractive index distribution of an object, which will be denoted as $n(\mathbf{r}) = 1 - \delta(\mathbf{r}) + i\beta(\mathbf{r})$, $i \equiv \sqrt{-1}$. All mathematical functions in this study will be assumed to be bounded and have compact support. Conventional image reconstruction methods for EIXPCT contain two steps. In the first step, phase-retrieval is performed at each tomographic view angle. Two tomographic data sets, also known as sinograms, are computed that permit $\delta(\mathbf{r})$ and $\beta(\mathbf{r})$ to be independently reconstructed by use of a reconstruction algorithm, such as the filtered backprojection (FBP) algorithm. To perform the phase-retrieval step, two or more distinct images are generally required to be acquired at each tomographic view angle [4]. This is undesirable for in-vivo imaging because it can increase imaging times and radiation dose. To circumvent this, single-shot methods have been proposed that can remove the need to acquire multiple images per view angle. However, previously proposed single-shot EIXPCT methods require restrictive assumptions regarding the scanning geometry [5] or object [6], or require use of an energy-sensitive detector [7].

In this work, a new single-shot method for EIXPCT is established that circumvents these assumptions. In the proposed method, the phase-retrieval and image reconstruction steps are combined into a single step. Estimates of $\delta(\mathbf{r})$ and $\beta(\mathbf{r})$ are computed directly from the single-shot tomographic measurement data by use of a non-linear joint reconstruction (JR) method as described below.

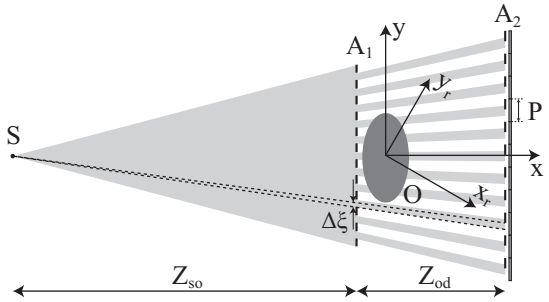

Fig. 1. An experimental set up. A_1 is the pre-sample mask and is placed before the sample. A_2 is the detector mask and is placed immediately before the detector with a pixel size P. S is the X-ray source. The distance between the source and A_1 is denoted as z_{so} and the distance between A_1 and the detector is denoted as z_{od}.

Consider a canonical EIXPCT system as depicted in Fig. 1 [2, 8]. The coordinate $\boldsymbol{r} = (x, y)$ describes a stationary reference coordinate system. The origin of the reference system corresponds to the assumed origin of tomographic scanning. A rotating coordinate system (x_r, y_r) will be utilized to describe the tomographic measurements and is related to the reference system as $x_r = x\cos\theta + y\sin\theta$, $y_r = y\cos\theta + x\sin\theta$. Here, θ denotes the tomographic view angle that is measured from the positive x-axis, y_r denotes the detector coordinate, and the positive x_r-axis denotes the direction of the incident of the X-

ray beam, assuming an incident X-ray plane-wave or spherical wave in the paraxial limit.

An aperture (pre-sample mask) denoted by A_1 is placed between the X-ray source S and the to-be-imaged object that is denoted by O. The distance from the source to A_1 is denoted as z_{so}. Another aperture (detector mask), denoted by A_2, is located immediately in front of the detector and is parallel to the pre-sample mask A_1 and is at a distance z_{od} from it. The relative positions of the two apertures along the y_r-axis can be changed by moving the pre-sample mask. Translating A_1 by $\Delta\xi$ results in the measurement of different deflected X-ray beam components. In this way, differential phase information is encoded in the measured X-ray wave intensity $I(\theta, y_r; \beta, \delta)$.

Let $\mathcal{H}$ denote the two-dimensional (2D) Radon transform operator that, when acting on $\beta(\mathbf{r})$, is defined as

$$p(\theta, y_r; \beta) \equiv \mathcal{H}\beta(\mathbf{r}) = \int_{L(y_r,\theta)} \beta(\boldsymbol{r}) dx_r, \tag{1}$$

where the path of integration $L(y_r, \theta)$ is a line that is parallel to x_r axis and goes through $(0, y_r)$. Similarly, let $\mathcal{D}$ denote the first-order derivative of the 2D Radon transform with respect to the detector coordinate y_r:

$$\mathcal{D}(\theta, y_r; \delta) \equiv \frac{\partial}{\partial y_r} p(\theta, y_r; \delta) = \frac{\partial}{\partial y_r} \int_{L(y_r,\theta)} \delta(\boldsymbol{r}) dx_r. \tag{2}$$

In terms of these quantities and assuming a monochromatic incident wavefield with wavelength λ, the EIXPCT imaging model can be expressed as [8]

$$I(\theta, y_r; \beta, \delta) = \exp\left(-\frac{2\pi}{\lambda} p(\theta, y_r; \beta)\right) I_{TC}\left(\Delta\xi - \frac{z_{od}}{M}\mathcal{D}(\theta, y_r; \delta)\right), \tag{3}$$

where $M \equiv (z_{so} + z_{od})/z_{so}$. The quantity $I_{TC}(\Delta\xi)$ represents the illumination curve that describes the relationship between the measured intensity and the aperture position when the object is absent and is typically acquired by a separate calibration procedure. In single-shot imaging, the aperture offset $\Delta\xi$ is fixed at a given tomographic view angle θ, as only a single image is recorded, but $\Delta\xi$ may vary between view angles. As such, the notation $\Delta\xi_\theta$ will be employed.

In practice, $\mathcal{D}(\theta, y_r; \delta)$ is often small enough for Eq. (3) to be linearized by use of a Taylor expansion [8] as

$$I(\theta, y_r; \beta, \delta) = \exp\left(-\frac{2\pi}{\lambda} p(\theta, y_r; \beta)\right) \times \left[I_{TC}(\Delta\xi_\theta) - \frac{z_{od}}{M} I'_{TC}(\Delta\xi_\theta)\mathcal{D}(\theta, y_r; \delta)\right], \tag{4}$$

where $I'_{TC}(\Delta\xi_\theta)$ denotes the first-order derivative of the illumination curve at aperture position $\Delta\xi_\theta$.

Next, in order to formulate image reconstruction in single-shot EIXPCT as a numerical optimization problem, the imaging model in Eq. (4) is discretized. Let the vectors $\boldsymbol{\beta} = [\beta_{1,1}, \beta_{1,2}, ..., \beta_{1,N_x}, \beta_{2,1}, ..., \beta_{N_x,N_y}]^T \in \mathbb{R}^N$ and $\boldsymbol{\delta} = [\delta_{1,1}, \delta_{1,2}, ..., \delta_{1,N_x}, \beta_{2,1}, ..., \delta_{N_x,N_y}]^T \in \mathbb{R}^N$ represent the values of $\beta(\mathbf{r})$ and $\delta(\mathbf{r})$ sampled at the $N = N_x N_y$ vertices $\boldsymbol{r}_{i,j} = (x_i, y_j)$ ($i = 1, 2, ..., N_x$ and $j = 1, 2, ..., N_y$) of a Cartesian grid. Consider that Q samples of the wavefield intensity corresponding to sampled values of y_r are acquired at each of P tomographic view angles. The vector $\boldsymbol{I}(\boldsymbol{\beta}, \boldsymbol{\delta}) \in \mathbb{R}^{PQ}$ contains a lexicographical ordering of these values. The notation $[\cdot]_i$ will be employed to denote the i-th component of the vector enclosed by the brackets.

Discrete representations of the 2D Radon transform and its first-order derivative will be denoted as $\boldsymbol{H} \in \mathbb{R}^{PQ\times N}$ and $\boldsymbol{D} \in \mathbb{R}^{PQ\times N}$, respectively. Finally, let $\boldsymbol{\Delta\xi} \in \mathbb{R}^P$ denote the collection of aperture offsets employed at the different tomographic view angles. Is should be noted that in previously proposed single-shot methods, the aperture offset was assumed to be fixed for all view angles. However, as described below, the proposed image reconstruction method will permit exploration of more general single-shot data-acquisition protocols in which the aperture offset varies with view angle. The quantity $[\boldsymbol{\Delta\xi}]_{\lceil \frac{i}{Q} \rceil}$ corresponds to the aperture offset employed at the tomographic view angle corresponding to the measurement $[\boldsymbol{I}(\boldsymbol{\beta}, \boldsymbol{\delta})]_i$, where $\lceil \frac{i}{Q} \rceil$ defines the smallest integer larger than $\frac{i}{Q}$. In terms of these quantities, a discrete version of the imaging model can be expressed as

$$[\boldsymbol{I}(\boldsymbol{\beta}, \boldsymbol{\delta})]_i = \exp\left(-\frac{2\pi}{\lambda}[\boldsymbol{H\beta}]_i\right) \times \left[I_{TC}([\boldsymbol{\Delta\xi}]_{\lceil \frac{i}{Q} \rceil}) - \frac{z_{od}}{M} I'_{TC}([\boldsymbol{\Delta\xi}]_{\lceil \frac{i}{Q} \rceil})[\boldsymbol{D\delta}]_i\right], \tag{5}$$

where $i = 1, 2, ..., PQ$.

Based on the discrete imaging model, JR of $\boldsymbol{\beta}$ and $\boldsymbol{\delta}$ can be formulated as a numerical optimization problem. Let $\boldsymbol{I}_m$ and $\boldsymbol{I}(\boldsymbol{\beta}, \boldsymbol{\delta})$ denote the measured intensity data and the intensity data simulated by use of Eq. (5) for a specified choice of $\boldsymbol{\delta}$ and $\boldsymbol{\beta}$, respectively. Penalized least squares estimates of $\boldsymbol{\delta}$ and $\boldsymbol{\beta}$ can be jointly determined as

$$(\tilde{\boldsymbol{\beta}}, \tilde{\boldsymbol{\delta}}) = \arg\min_{\tilde{\boldsymbol{\beta}}, \tilde{\boldsymbol{\delta}}} ||\boldsymbol{I}_m - \boldsymbol{I}(\tilde{\boldsymbol{\beta}}, \tilde{\boldsymbol{\delta}})||^2 + R(\tilde{\boldsymbol{\beta}}, \tilde{\boldsymbol{\delta}}), \tag{6}$$

where $R(\tilde{\boldsymbol{\beta}}, \tilde{\boldsymbol{\delta}})$ is a penalty function that imposes regularization on the estimates. The first term in the objective function in Eq. (6) - the data fidelity term - is non-convex. However, as demonstrated below, this will not prevent accurate image reconstruction. In this work, the penalty function was taken to be of the form $R(\tilde{\boldsymbol{\beta}}, \tilde{\boldsymbol{\delta}}) = l_1 R_\beta(\tilde{\boldsymbol{\beta}}) + l_2 R_\delta(\tilde{\boldsymbol{\delta}})$, where l_1 and l_2 denote regularization parameters, and $R_\beta(\tilde{\boldsymbol{\beta}})$ and $R_\delta(\tilde{\boldsymbol{\delta}})$ are differentiable functions.

The gradients of the objective function $f(\tilde{\boldsymbol{\beta}}, \tilde{\boldsymbol{\delta}})$ with respect to the vectors $\tilde{\boldsymbol{\beta}}$ and $\tilde{\boldsymbol{\delta}}$ are given by

$$\nabla_{\tilde{\boldsymbol{\beta}}} f(\tilde{\boldsymbol{\beta}}, \tilde{\boldsymbol{\delta}}) = 2\boldsymbol{I}'^*_{\tilde{\boldsymbol{\beta}}}(\boldsymbol{I}(\tilde{\boldsymbol{\beta}}, \tilde{\boldsymbol{\delta}}) - \boldsymbol{I}_m) + l_1 \nabla_{\tilde{\boldsymbol{\beta}}} R_\beta(\tilde{\boldsymbol{\beta}}), \tag{7}$$

$$\nabla_{\tilde{\boldsymbol{\delta}}} f(\tilde{\boldsymbol{\beta}}, \tilde{\boldsymbol{\delta}}) = 2\boldsymbol{I}'^*_{\tilde{\boldsymbol{\delta}}}(\boldsymbol{I}(\tilde{\boldsymbol{\beta}}, \tilde{\boldsymbol{\delta}}) - \boldsymbol{I}_m) + l_2 \nabla_{\tilde{\boldsymbol{\delta}}} R_\delta(\tilde{\boldsymbol{\delta}}), \tag{8}$$

where $\boldsymbol{I}'^*_{\tilde{\boldsymbol{\beta}}} \in \mathbb{R}^{N\times PQ}$ and $\boldsymbol{I}'^*_{\tilde{\boldsymbol{\delta}}} \in \mathbb{R}^{N\times PQ}$ denote the adjoint operators corresponding to the derivatives of $\boldsymbol{I}(\tilde{\boldsymbol{\beta}}, \tilde{\boldsymbol{\delta}})$ with respect to $\tilde{\boldsymbol{\beta}}$ and $\tilde{\boldsymbol{\delta}}$, respectively. The adjoint operators, applied to a small vector $\boldsymbol{\epsilon} \in \mathbb{R}^{PQ}$, can be computed as

$$\boldsymbol{I}'^*_{\tilde{\boldsymbol{\beta}}}\boldsymbol{\epsilon} = -\frac{2\pi}{\lambda}\boldsymbol{H}^*\boldsymbol{x} \text{ and } \boldsymbol{I}'^*_{\tilde{\boldsymbol{\delta}}}\boldsymbol{\epsilon} = -\boldsymbol{D}^*\boldsymbol{y}, \tag{9}$$

where

$$[\boldsymbol{x}]_i = \left(I_{TC}([\boldsymbol{\Delta\xi}]_{\lceil \frac{i}{Q} \rceil}) - \frac{z_{od}}{M} I'_{TC}([\boldsymbol{\Delta\xi}]_{\lceil \frac{i}{Q} \rceil})[\boldsymbol{D\tilde{\delta}}]_i\right) \times \exp\left(-\frac{2\pi}{\lambda}[\boldsymbol{H\tilde{\beta}}]_i\right)\boldsymbol{\epsilon}_i, \tag{10}$$

$$[\boldsymbol{y}]_i = \frac{z_{od}}{M} I'_{TC}([\boldsymbol{\Delta\xi}]_{\lceil \frac{i}{Q} \rceil}) \exp\left(-\frac{2\pi}{\lambda}[\boldsymbol{H}(\tilde{\boldsymbol{\beta}})]_i\right)\boldsymbol{\epsilon}_i,\ i = 1, 2, ..., PQ. \tag{11}$$

A batch gradient algorithm is proposed for solving Eq. (6). Pseudocode for the algorithm is provided in Algorithm 1. The iteration stops when the objective function value falls below a specified threshold.

Algorithm 1. JR of $\tilde{\beta}$ and $\tilde{\delta}$ using a batch gradient algorithm

Calibrate the illumination curve
Read in measured data I
Initialization: $\tilde{\beta}^{(0)} \leftarrow 0; \tilde{\delta}^{(0)} \leftarrow 0; k \leftarrow 0$
while stopping criterion is not satisfied **do**
  $k \leftarrow k+1$
  Calculate the intensity data $\boldsymbol{I}(\tilde{\beta}^{(k)}, \tilde{\delta}^{(k)})$
  Compute cost $||\boldsymbol{I}_m - \boldsymbol{I}(\tilde{\beta}^{(k)}, \tilde{\delta}^{(k)})||^2 + R(\tilde{\beta}^{(k)}, \tilde{\delta}^{(k)})$
  $\boldsymbol{d}_\beta \leftarrow -\nabla_\beta ||\boldsymbol{I}_m - \boldsymbol{I}(\tilde{\beta}^{(k)}, \tilde{\delta}^{(k)})||^2 + l_1 \nabla_\beta R_{TV}(\tilde{\beta}^{(k)})$ ▷ ∇_β denotes the derivative w.r.t. $\tilde{\beta}$
  $\boldsymbol{d}_\delta \leftarrow -\nabla_\delta ||\boldsymbol{I}_m - \boldsymbol{I}(\tilde{\beta}^{(k)}, \tilde{\delta}^{(k)})||^2 + l_2 \nabla_\delta R_{TV}(\tilde{\delta}^{(k)})$ ▷ ∇_δ denotes the derivative w.r.t. $\tilde{\delta}$
  $(\tilde{\beta}^{(k+1)}, \tilde{\delta}^{(k+1)}) \leftarrow (\tilde{\beta}^{(k)}, \tilde{\delta}^{(k)}) + \tau(\boldsymbol{d}_\beta, \boldsymbol{d}_\delta)$ ▷ τ is the step size obtained by a line search method

Computer-simulation studies were first conducted to demonstrate the feasibility of achieving accurate JR of β and δ from idealized noiseless measurements by use of Algorithm 1. The numerical phantoms shown in Figs. 2a and 2b were employed to represent β and δ. The phantoms contained 256×256 pixels of size $100\,\mu m \times 100\,\mu m$ and the values of β and δ were representative of soft tissue. Both phantoms contained multiple materials.

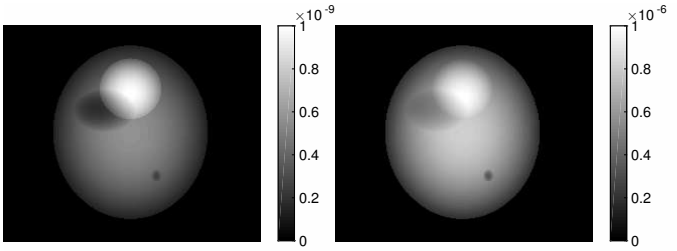

Fig. 2. Numerical phantoms utilized to represent (a) β and (b) δ in the computer-simulation studies.

Noiseless simulated intensity data were computed by use of Eq. (3). At each view angle, 400 samples of the wavefield intensity were specified along the detector array. The illumination curve was modeled after experimental measurements [5]. It was specified as a Gaussian distribution $I_{TC} = 0.13 + 0.87\exp(-\Delta\xi^2/1.84 \times 10^{-10})$, where $\Delta\xi$ has units of m and I_{TC} has arbitrary units. The offset $\Delta\xi$ was specified as $\Delta\xi = 9.6\ \mu m$, as $\Delta\xi \pm 9.6\ \mu m$ corresponded to the locations of largest derivative of the illumination curve. The imaging parameters were: $z_{so} = 1.6$ m, $z_{od} = 0.4$ m, $\lambda = 10^{-10}$ m.

Two distinct single-shot EIXPCT data sets were computed using the methodology described above. The first data set was a conventional single-shot data in which the aperture offset was constant at 720 evenly spaced view angles that spanned a 2π angular range; this data set will be referred to as the constant aperture position (CAP) plan. The offset value was $\Delta\xi = 9.6\ \mu m$. The second single-shot data set was non-conventional and its design was motivated by the flexibility of the proposed JR method. In this data set, referred to as the alternating aperture position (AAP) plan, intensity data were collected at 360 evenly spaced view angles that spanned a π angular range. However, instead of keeping the aperture offset fixed, it was alternated between $\Delta\xi = 9.6\ \mu m$ and $\Delta\xi = -9.6\ \mu m$, changing value at every view angle. The AAP plan addresses the situation when single-shot measurements are not available over a complete 2π range. Images were reconstructed from both data sets by use of Algorithm 1 with $l_1 = l_2 = 0$ (i.e., no regularization).

The reconstructed images and image profiles corresponding

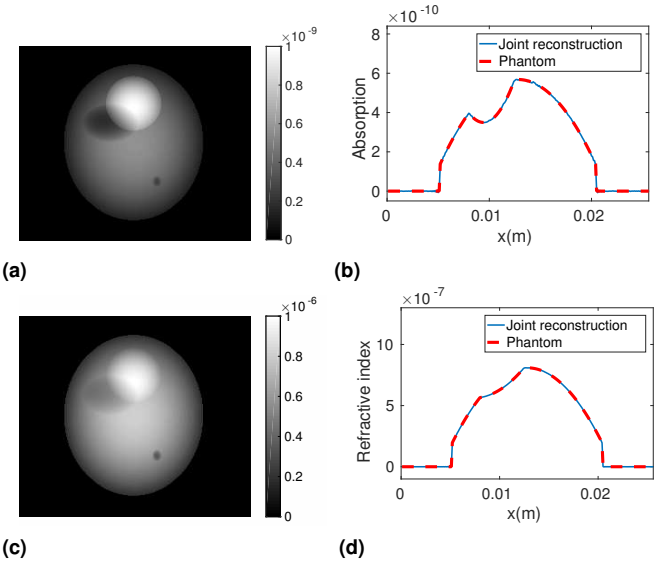

Fig. 3. Computer-simulation results corresponding to the CAP plan. Reconstructed estimates of β (MSE = 1.8×10^{-24}) and δ (MSE = 1.3×10^{-19}) are shown in subfigures (a) and (c). Line profiles through the reconstructed images and corresponding true phantoms are shown in subfigures (b) and (d).

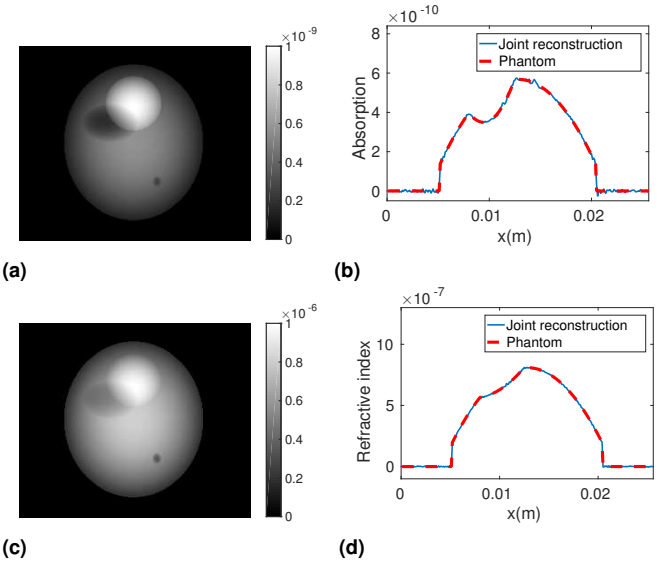

Fig. 4. Computer-simulation results corresponding to the AAP plan. Reconstructed estimates of β (MSE = 3.5×10^{-23}) and δ (MSE = 7.5×10^{-18}) are shown in subfigures (a) and (c). Line profiles through the reconstructed images and corresponding true phantoms are shown in subfigures (b) and (d).

to the CAP plan are shown in Figs. 3. These results confirm that the JR algorithm can reconstruct highly accurate images from idealized single-shot data. A similar observation holds true for the AAP plan results shown Fig. 4. The AAP plan results suggest, for the first time, that a full 2π angular scanning range can be traded for a reduced scanning range of (at least) π if additional diversity in the measured data are created by varying the aperture offset as a function of view angle.

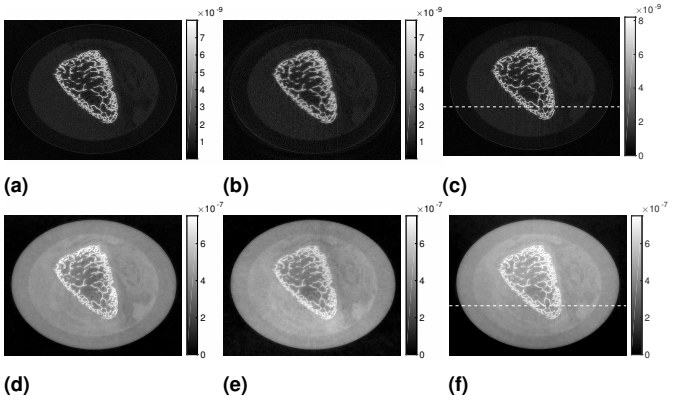

Fig. 5. Estimates of β (top row) and δ (bottom row) that were jointly reconstructed from the (a),(d) CAP data set, and (b),(e) AAP data set. The corresponding estimates obtained by use of the conventional two-step method are shown in subfigures (c) and(d).

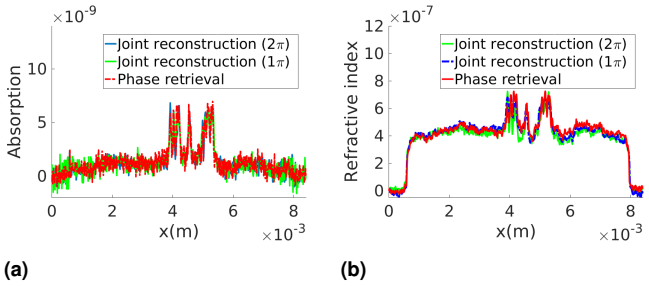

Fig. 6. Profiles through the reconstructed images for all data acquisition plans at the white dashed line indicated in Figs. 5c and 5f. The profiles corresponding to the estimates of β and δ are shown in subfigures (a) and (b), respectively.

To demonstrate the value of the JR method under realistic conditions, studies that utilized experimental EIXPCT data sets were conducted. The experimental data were acquired in a previous study [5]. The imaged sample corresponded to a chicken bone and the mean X-ray energy was 17 keV. Addition details regarding the imaging system and imaging parameters can be found in reference [5]. As in the computer-simulation studies, intensity data were acquired at 720 view angles that were uniformly distributed over a 2π angular range. At each view angle, two intensity measurements were acquired corresponding to approximately symmetric positions on the illumination curve. A CAP data set was formed by retaining the measurements corresponding to one side of the illumination curve. An AAP data set was formed by keeping either the measurement corresponding to the positive or negative side of the illumination curve, in an alternating fashion as a function of view angle. Images were reconstructed from the CAP and AAP data sets by use of Algorithm 1. The penalty functions $R_\beta(\tilde{\beta})$ and $R_\delta(\tilde{\delta})$ were specified as a smoothed version of the total variation semi-norm [9]. Suitable values of the regularization parameters l_2 and l_1 were manually determined and fixed for use with both data sets. Images were also reconstructed by use of a conventional (non-single-shot) approach in which both images acquired at each view angle were employed to perform phase-retrieval, followed by application of the FBP algorithm to determine estimates of β and δ [5]. In this case, a π angular scanning range was utilized. In all cases, the pixel size of the reconstructed images was 9.9 μm.

The reconstructed images and corresponding image profiles reconstructed from the experimental data sets are displayed in Figs. 5 and 6. In all of the reconstructed images, the features of the bone structure can be clearly identified. Moreover, as evident from the nearly overlapping image profiles, the images reconstructed from the CAP and AAP single-shot data sets by use of the JR method are close in quantitative value to those reconstructed by use of the conventional two step approach.

In summary, a new JR method was proposed for single-shot EIXPCT. The proposed JR method, in effect, combines the phase-retrieval and image reconstruction steps into one. The JR method was formulated as a numerical optimization problem and a gradient-based algorithm was developed for its solution. The proposed method possesses advantages over previously-proposed single-shot methods for EIXPCT. The method does not require the assumption of a single material object [6]. Moreover, it does not require a parallel-beam geometry [5] and can be applied to the case of a cone-beam geometry where the incident beam divergence must be considered. Additionally, the method does not require use of an energy-sensitive detector [7] and can be employed with readily available integrating X-ray detectors. Finally, the flexibility of the method permits exploration of innovative data-acquisition protocols for single-shot EIXPCT, such as the AAP plan, which can relax requirements on the range of angular scanning. Additional studies are required to comprehensively evaluate the numerical and statistical properties of the method.

This work was supported in part by NIH award EB02060401 and NSF award CBET1263988.

REFERENCES

1. C. Hagen, P. Munro, M. Endrizzi, P. Diemoz, and A. Olivo, Medical physics **41**, 070701 (2014).
2. C. K. Hagen, P. C. Diemoz, M. Endrizzi, L. Rigon, D. Dreoosi, F. Arfelli, F. C. Lopez, R. Longo, and A. Olivo, "Quantitative edge illumination X-ray phase contrast tomography," in "SPIE Optical Engineering+ Applications," (International Society for Optics and Photonics, 2014), pp. 921205–921205.
3. C. Hagen, P. Diemoz, M. Endrizzi, L. Rigon, D. Dreossi, F. Arfelli, F. Lopez, R. Longo, and A. Olivo, Optics express **22**, 7989 (2014).
4. P. R. Munro, K. Ignatyev, R. D. Speller, and A. Olivo, Proceedings of the National Academy of Sciences **109**, 13922 (2012).
5. C. K. Hagen, M. Endrizzi, P. C. Diemoz, and A. Olivo, Journal of Physics D: Applied Physics **49**, 255501 (2016).
6. P. C. Diemoz, F. A. Vittoria, C. K. Hagen, M. Endrizzi, P. Coan, E. Brun, U. H. Wagner, C. Rau, I. K. Robinson, A. Bravin, and A. Olivo, Journal of synchrotron radiation **22**, 1072 (2015).
7. M. Das and Z. Liang, Optics letters **39**, 6343 (2014).
8. P. R. Munro, C. K. Hagen, M. B. Szafraniec, and A. Olivo, Optics express **21**, 11187 (2013).
9. E. Y. Sidky, C.-M. Kao, and X. Pan, Journal of X-ray Science and Technology **14**, 119 (2006).

FULL REFERENCES

1. C. Hagen, P. Munro, M. Endrizzi, P. Diemoz, and A. Olivo, "Low-dose phase contrast tomography with conventional X-ray sources," Medical physics **41**, 070701 (2014).
2. C. K. Hagen, P. C. Diemoz, M. Endrizzi, L. Rigon, D. Dreoosi, F. Arfelli, F. C. Lopez, R. Longo, and A. Olivo, "Quantitative edge illumination X-ray phase contrast tomography," in "SPIE Optical Engineering+ Applications," (International Society for Optics and Photonics, 2014), pp. 921205–921205.
3. C. Hagen, P. Diemoz, M. Endrizzi, L. Rigon, D. Dreossi, F. Arfelli, F. Lopez, R. Longo, and A. Olivo, "Theory and preliminary experimental verification of quantitative edge illumination X-ray phase contrast tomography," Optics express **22**, 7989–8000 (2014).
4. P. R. Munro, K. Ignatyev, R. D. Speller, and A. Olivo, "Phase and absorption retrieval using incoherent X-ray sources," Proceedings of the National Academy of Sciences **109**, 13922–13927 (2012).
5. C. K. Hagen, M. Endrizzi, P. C. Diemoz, and A. Olivo, "Reverse projection retrieval in edge illumination X-ray phase contrast computed tomography," Journal of Physics D: Applied Physics **49**, 255501 (2016).
6. P. C. Diemoz, F. A. Vittoria, C. K. Hagen, M. Endrizzi, P. Coan, E. Brun, U. H. Wagner, C. Rau, I. K. Robinson, A. Bravin, and A. Olivo, "Single-image phase retrieval using an edge illumination X-ray phase-contrast imaging setup," Journal of synchrotron radiation **22**, 1072–1077 (2015).
7. M. Das and Z. Liang, "Spectral X-ray phase contrast imaging for single-shot retrieval of absorption, phase, and differential-phase imagery," Optics letters **39**, 6343–6346 (2014).
8. P. R. Munro, C. K. Hagen, M. B. Szafraniec, and A. Olivo, "A simplified approach to quantitative coded aperture X-ray phase imaging," Optics express **21**, 11187–11201 (2013).
9. E. Y. Sidky, C.-M. Kao, and X. Pan, "Accurate image reconstruction from few-views and limited-angle data in divergent-beam CT," Journal of X-ray Science and Technology **14**, 119–139 (2006).